Direct internal methane reforming in biogas fuelled solid oxide fuel cell; the influence of operating parameters

Saadabadi, S. Ali; Illathukandy, Biju; Aravind, Purushothaman Vellayani

Important note
To cite this publication, please use the final published version (if applicable).
Please check the document version above.

RESEARCH ARTICLE

Direct internal methane reforming in biogas fuelled solid oxide fuel cell; the influence of operating parameters

S. Ali Saadabadi[1] | Biju Illathukandy[2,3] | Purushothaman Vellayani Aravind[1,4]

[1]Faculty of 3ME, Department of Process and Energy, Delft University of Technology, Delft, The Netherlands

[2]Centre for Rural Development & Technology, Indian Institute of Technology Delhi, New Delhi, India

[3]Mechanical Engineering, Government Engineering College Kozhikode, Kozhikode, India

[4]Energy and Sustainability Research Institute, Groningen University, Groningen, The Netherlands

Correspondence
S. Ali Saadabadi, Faculty of 3ME, Department of Process and Energy, Delft University of Technology, Leeghwaterstraat 39, 2628 CB Delft, The Netherlands.
Email: s.a.saadabadi@tudelft.nl

Abstract

Internal dry reforming (IDR) of methane for biogas-fed solid oxide fuel cell (SOFC) applications has been experimentally investigated on planar Ni-GDC (cermet anode) electrolyte-supported cells. This study focuses on the effect of CO_2 concentration, current density, operating temperature, and residence time on internal methane dry reforming. A single cell is fed with different CH_4/CO_2 mixture ratios between 0.6 and 1.5. Extra CO_2 recovered from carbon capture plants can be utilized here as a reforming agent. The I-V characterization curves are recorded at different operating conditions in order to determine the best electrochemical performance while the power production is maximized, and carbon deposition is suppressed. The outlet gas from the anode is analyzed by a micro gas chromatograph to investigate methane conversion inside the anode fuel channel and to understand its influence on the cell performance. Relatively long-term experiments have been performed for all gas mixtures at 850°C under a current density of 2000 A m^{-2}. The results indicate that when the cell is fed with biogas with an equimolar amount of CH_4 and CO_2, carbon deposition is prevented, and maximum power density is obtained.

KEYWORDS
biogas fuelled SOFC, internal dry reforming, solid oxide fuel cell, waste to energy

1 | INTRODUCTION

Waste to energy conversion is one of the most important technology to improve sustainability as it simultaneously reduces the fossil fuel consumption and greenhouse gas emission. High concentration of nutrients in wastewater streams is interesting for energy recovery.[1] Waste stream contains organic compounds that can be converted to biogas through anerobic digestion (AD) process.[2] Biogas consists of methane, carbon dioxide, and traces of contaminants like hydrogen sulfide and volatile organic compounds (VOCs).[3-6] Biogas produced is commonly flared in conventional wastewater treatment plants (WWTPs) hence increasing greenhouse gas emissions.[7] For the large-scale WWTPs, an internal combustion

(IC) engine can be used to produce heat and power simultaneously in combined heat and power (CHP) systems.[8] Based on AD conditions and the source of the wastewater stream, the concentration of methane is in the range of 50-70 mol.% and this might be different for different seasons due to different ambient temperatures.[9,10] High concentration of CO_2 brings down the energy density of biogas fuel which leads to power de-rating of biogas fuelled IC engine.[11] Moreover, fluctuation of methane concentration also influences the IC engine performance and NOx emission is significantly high at high combustion temperature.[12]

Replacing the IC engine with Solid Oxide Fuel cell (SOFC) can improve the power production and makes the whole system more sustainable in terms of energy efficiency

TABLE 1 Overview of some of experimental studies on internal dry reforming of biogas in SOFC

Cell anode material	Temperature (°C)	Cell type/size	Current density/ Potential	Fuel	Ref.
Ni-ScSZ (ASC)	800	Button cell	5000 & 2000 (A m^{-2}) 2000 A m^{-2}	Actual biogas Simulated ($R = 1.5$)	[27]
Ni-GDC (ESC) Ni-YSZ (ASC)	850	Circular cell ($D = 80$ mm)	3000 A m^{-2} 5000 A m^{-2}	$R = 0.55$ $R = 0.67$	[28]
Ni-YSZ Ni-GDC	875 700	Noncommercial	0.45 V 0.45 V	$R = 1.0$	[29]
Ni-YSZ	875	Button cell (noncommercial)	1300 A m^{-2}	$R = 1.0$	[30]
Ni–YSZ (ASC)	800	Button cell	4000-16 000 A m^{-2}	$R = 3.0$	[31]
Ni-YSZ	850	Tubular cell	0.7 V	$R = 0.82$	[32]
Ni/YSZ (ASC)	800	Tubular cell	1600 A m^{-2}	$R = 0.43$	[33]
Ni(Au)-GDC	600-640	Tubular cell	Up to 2000 A m^{-2}	$R = 1.0$	[34]
Ni-YSZ (ASC)	800	Circular cell ($D = 56$ mm)	1600 A m^{-2}-0.6 V	$R = 1$ with 6% humidity	[35]

and emission levels.[13] SOFCs are more efficient and fuel flexible in comparison with IC engines.[14] However, biogas should be reformed to a hydrogen-rich gas either internally or externally for a biogas-SOFC system.[15] SOFC can tolerate high concentration of CO_2 because this is not a toxic gas for SOFCs. Additionally, it aids methane dry reforming reaction at high operating temperatures.[16] The R ratio is defined as the partial pressure of CH_4 to CO_2 ($R = CH_4/CO_2$) and indicates the amount of dry reforming agent (CO_2) present in the biogas. The R ratio may change at different biogas production conditions. On the other hand, concentrations of H_2S and other contaminants such as siloxanes in biogas should be reduced to a few ppm levels (even less than 0.5 ppm).[17-19] High concentration of contaminants has an influence on the electrochemical performance and increases the cell degradation rate. Using a gas cleaning unit is essential for biogas-SOFC systems.[20,21]

Internal reforming is more efficient and cost-effective method in comparison with external reforming.[22,23] Generated heat through the electrochemical reactions of fuel is used for the endothermic reforming reactions, which decreases the cooling demand of SOFC stack.[23,24] However, some challenges such as slow kinetics, high thermal stresses, and risk of carbon deposition make this a complex method.[25] There are relatively few research studies on biogas fuelled SOFCs specifically operating under internal reforming conditions, with limited experimental investigations on dry reforming.[26]

Shiratori et al[27] have used actual biogas (with R fluctuating between 1.4 and 1.9) and simulated biogas ($R = 1.5$) fuels for Ni-ScSZ button cell. No carbon deposition was observed for the simulated biogas under a current density of 2000 A m^{-2} whereas, severe carbon deposition took place during the long-term experiment with actual biogas. Lanzini and Leone[28] have recommended using an extra 1.2 mole of CO_2 to each mole

of biogas ($R = 0.55$) in order to achieve a stable voltage in biogas-dry reforming for Ni-GDC (ceramic-metallic composite) electrolyte-supported cell (ESC) at a current density of 3000 A m^{-2}. The same experiment has been conducted for a Ni-YSZ anode supported cell (ASC) and the operating condition with $R = 0.67$ at a current density of 5000 A m^{-2} has been advised. An equimolar CH_4/CO_2 feed gas composition ($R = 1$) is recommended by Yentekakis et al[29] to maximize the electrical power output for Ni-YSZ and Ni-GDC SOFC at 875 and 700°C, respectively. This maximum power is achieved at a cell voltage of 0.450 V. In this study, a noncommercial cell was designed with an electrolyte tube with a thin film coated inside (anode) and outside (cathode) of the tube. On the other hand, a negligible carbon deposition has been observed by Goula et al[30] for the methane dry reforming experiments with $R > 1.0$ performed for a Ni-YSZ anode supported cell in open-circuit voltage (OCV) condition at 800°C. The stability (stable voltage at constant current density) of an ASC with Ni-YSZ anode was studied for rich-methane biogas ($R = 3.0$).[31] The stability was improved by increasing the CO_2 concentration by 20% and the operating current density (CD) to 16 000 A m^{-2}. It has also been reported that adding CO_2 to general biogas composition decreases the operating voltage of the cell which results in reduced system efficiency.[31] Staniforth and Ormerod[32] have studied the impact of methane concentrations on the performance of a small tubular SOFC with Ni-YSZ anode. They found that at a methane concentration of 45% ($R = 0.82$), the obtained power was maximum corresponding to the high concentration of H_2 and CO through internal dry reforming at 850°C. Direct internal dry reforming of biogas in a tubular (Ni-YSZ anode) SOFC was performed with different R ratios of 0.43, 0.32, and 0.25 where the number of moles of CO_2 was varied. Performance maps of the SOFC for a wide range of current densities under different fuel flow rates were determined. It is claimed that dry

reforming is more effective for an *R*-value of 0.43.[33] The results of these experimental studies are summarized in Table 1.

There are also some studies carried out to evaluate the effect of CO_2 partial pressure on dry reforming reaction for different catalysts. Xu et al[36] proposed an *R* ratio of 0.77 as an optimum gas composition for dry reforming over a Ni-Co bimetallic catalyst. It is claimed that a higher amount of CO_2 is not beneficial in preventing gradual catalyst deactivation and it might increase the risk of Ni re-oxidation.[37] Guerra et al[38] have assessed dry reforming on Ni/YSZ catalyst. A range of $0.5 < R < 0.75$ has been suggested to obtain a high methane conversion and prevent carbon deposition. These contradictory recommendations for operating SOFC under internal biogas reforming conditions have shown that further experimental investigations are required, especially for the Ni-GDC anode.

Ni-GDC as an anode has certain advantages when used in the biogas-SOFC system. This type of SOFC anode shows better performance under methane dry reforming in comparison to Ni-YSZ anode because of its higher ionic and electronic conductivity.[29] Also, Ni-GDC can tolerate higher levels of H_2S contamination (2 ppm) which can be present at the outlet of the biogas gas cleaning unit (GCU).[39] Zhang et al[40] examined the impact of sulfur poisoning on the operational behavior of Ni-YSZ and Ni-GDC cermet anodes. The results revealed that Ni/GDC cermet anode exhibited better electrochemical performance during the exposure to H_2S-containing gas. The GDC can still support the electrochemical reactions while the Ni surface is blocked due to H_2S poisoning. This is attributed to mixed ionic-electronic conductivity and better hydrogen adsorption on the anode surface.[41] It is also observed that sulfur poisoning is slower during dry methane reforming in comparison with steam methane reforming.[42,43]

The objective of this research is to experimentally explore the influence of the SOFC operating conditions on direct internal dry reforming and the electrochemical performance of cell. The experimental study with a commercial Ni-GDC anode, electrolyte-supported cell is conducted at different operating temperatures (800-900°C). The impact of fluctuation of CH_4/CO_2 ratio (due to the biogas production conditions) on the methane reforming and the cell electrochemical performance is studied. Additionally, the influence of the current density in suppressing carbon deposition, which is predicted through the thermochemical equilibrium calculations, is evaluated. The relatively long-term experimental study presented here investigates the optimum and safe operating conditions in terms of both power production and in preventing carbon deposition.

2 | BIOGAS REFORMING

In biogas-SOFC systems, methane should be reformed to provide H_2 and CO, since direct electrochemical oxidation of methane does not practically contribute to the power generation.[11,44] External steam reforming technique is commonly used for biogas-SOFC systems in order to provide an appropriate fuel, which increases the cost and complexity of the biogas-SOFC systems.[45,46] Through an external steam reforming unit, hydrogen-rich gas is produced for the electrochemical reaction on the anode side (Equation 1). Due to the high operating temperature of SOFCs and existence of appropriate catalysts (eg, Ni), internal reforming of methane is also feasible. However, carbon deposition is still a challenge.[35] Carbon deposition can limit the cell catalytic properties and increase the cell polarization caused by anode structure damage.[47] Steam reforming also takes place in direct internal reforming (DIR) of methane. In this case, a high concentration of steam is required to be mixed with biogas. Steam to carbon ratio (SC) between 0.5 and 4 (on a molar basis) is proposed in order to prevent the carbon deposition.[20,48,49] On the other hand, the high concentration of steam decreases the energy density of mixed fuel and dilutes the H_2 and CO concentrations. Furthermore, generation of the high-temperature steam is an energy-demanding process and reduces the overall efficiency of the whole system.[50]

$$CH_4 + H_2O \leftrightarrow 3H_2 + CO, \quad \Delta H^0_{T=298} = 206 \text{ kJ mol}^{-1} \quad (1)$$

It is possible to take advantage of the high concentration of CO_2 in biogas to reform methane through internal dry reforming (IDR).[51] In this case, one greenhouse gas (CO_2) is used to reform another greenhouse gas (CH_4) into hydrogen and CO and this helps in reducing the CO_2 emission per kWh power generation (Equation 2). For instance, the impact of the dry reforming reaction on methane conversion is more dominant when SC ratios is lower than 3 in a biogas combined reforming.[52] Ni anode is also an appropriate catalyst for IDR.[34,53]
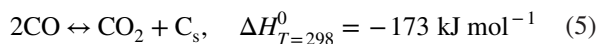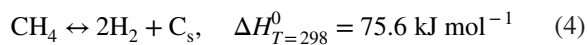
$$CH_4 + CO_2 \leftrightarrow 2H_2 + 2CO, \quad \Delta H^0_{T=298} = 247 \text{ kJ mol}^{-1} \quad (2)$$
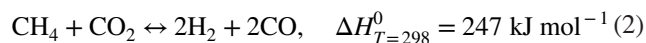
Dry reforming is a highly endothermic reaction that causes thermal stress on the cell, possibly resulting in cell cracking.[31] The H_2/CO ratio in the products of methane dry reforming is less than that of steam reforming (Equation 1). In operating SOFC (under a current density), steam and CO_2 are produced through the electrochemical reactions of hydrogen and CO in the anode fuel channel. In the presence of these gas species at high temperature, the reverse water gas shift (RWGS) reaction also takes place simultaneously (Equation 3).

$$H_2 + CO_2 \leftrightarrow CO + H_2O, \quad \Delta H^0_{T=298} = 41 \text{ kJ mol}^{-1} \quad (3)$$

The RWGS reaction is sensitive to temperature. Due to the moderate endothermic nature of this reaction, high hydrogen conversion is thermodynamically favored at higher

temperatures. So, when the temperature is above 830°C, it results in a higher CO concentration in the gas mixture.[54,55]

One of the major concerns of biogas-SOFC operation with IDR is the high risk of carbon deposition since the Ni is an active catalyst, which promotes carbon formation as well. From the thermodynamics point of view, for biogas-SOFC, carbon deposition is predicted for SOFC operating at OCV even at very high operating temperature (900°C). The carbon deposition within the SOFC operation temperature range (600-1000°C) is in the form of graphite.[47] In the case of DIR of biogas, steam reforming is more effective than dry reforming in preventing carbon deposition. Even though adding CO_2 as a reforming agent to the SOFC fuel increase the concentration of oxygen (to reform methane), on the other hand, it increases the concentration of carbon in the fuel. The high concentration of CO_2 is more susceptible to coking.[56,57] However, using CO_2 for methane reforming is an effective technique to reduce greenhouse gas emission. Carbon deposition leads to cell degradation because of catalyst deactivation of anode. This can happen through the following reactions.

$$CH_4 \leftrightarrow 2H_2 + C_s, \quad \Delta H^0_{T=298} = 75.6 \text{ kJ mol}^{-1} \quad (4)$$

$$2CO \leftrightarrow CO_2 + C_s, \quad \Delta H^0_{T=298} = -173 \text{ kJ mol}^{-1} \quad (5)$$

Formed carbon can fill in the pores and destroy the support of the anode catalyst which also can lead to anode delamination.[38,58] High concentration of steam in inlet gas fuel can suppress the rate of carbon deposition or carbon removal through the following reaction that is not the case in IDR at open-circuit voltage (OCV).

$$H_2O + C_s \leftrightarrow CO + H_2, \quad \Delta H^0_{T=298} = 131 \text{ kJ mol}^{-1} \quad (6)$$

3 | THERMODYNAMIC APPROACH

Cell voltage depends on the mole fractions of reactants (H_2 and CO) and products (H_2O and CO_2) at the inlet and outlet of the fuel channel. The Nernst voltage is calculated based on oxygen partial pressure in the anode and cathode sides (Equation 7).[10]

$$V_{\text{Nernst}} = \frac{RT}{nF} \ln \left(\frac{Po_{2cat}}{Po_{2ano}} \right) \quad (7)$$

where R is the universal gas constant, T (K) is the cell operating temperature, F is the Faraday constant and n is the number of O_2 electrons participating in the electrochemical reactions ($n = 4$). The partial pressure of the oxygen in the cathode side is 0.21 as air is fed to the cathode side, and the oxygen partial pressure
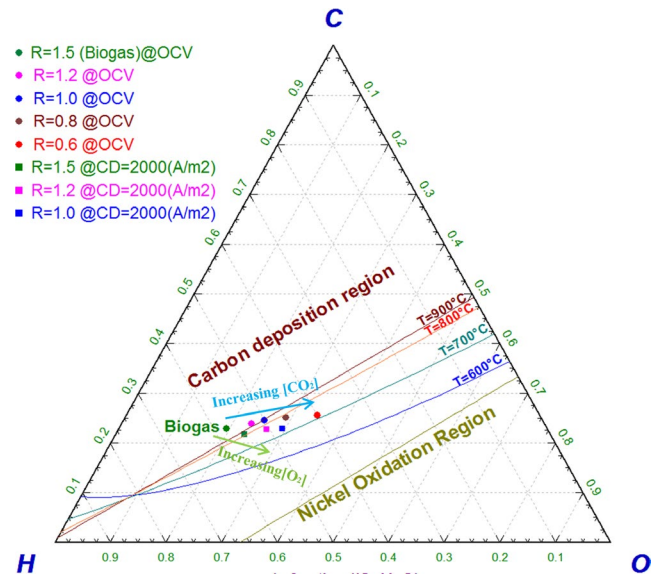

FIGURE 1 Carbon deposition limits in a C-H-O ternary diagram based on equilibrium calculation at atmospheric pressure

for the anode side depends on the biogas composition and it is calculated based on the equilibrium condition by FactSage software (V. 5.4.1, Thermfact/CRCT and GTT-Technologies).

The cell efficiency is defined to evaluate the cell performance for different type of fuel and various operating temperature. The efficiency is calculated based on the operating voltage and the maximum electrical work (the Gibbs free energy $\Delta \overline{g}_f$) as shown in Equation (8),[59] where the term of $\left(\Delta \overline{g}_f / n \cdot F \right)$ is the maximum cell voltage possible for the fuel and V_{cell} is the cell operating voltage

$$\eta_{cell} = V_{cell} / \left(\Delta \overline{g}_f / n \cdot F \right) \quad (8)$$

The maximum cell efficiency ($V_{\text{cell}} = V_{\text{Nernst}}$) for hydrogen fed SOFC operating at 850°C (LHV (lower heating value) based with $\Delta \overline{h}_f = 248.5 \text{ kJ mol}^{-1}$) is around 75% and this decreases with a drop in the cell operating voltage.

The carbon deposition threshold can be predicted by thermodynamic calculations at equilibrium condition. Thus, the C-H-O ternary diagram for different gas compositions with different CH_4 / CO_2 molar ratios (R) and operating temperatures have been illustrated in Figure 1. Increasing the operating temperature and concentration of CO_2 can decrease the risk of carbon deposition. The circular points in Figure 1 show the fuel cell operating condition at OCV (assuming no oxygen transfers from cathode to anode). At closed-circuit operating conditions, oxygen ions transfer through the electrolyte layer. Steam and carbon dioxide are produced on the anode side due to the electrochemical reactions of hydrogen and carbon monoxide. These products can again contribute to the methane reforming reactions (Equations 1 and 2). This can prevent carbon deposition to some extent (square

points in Figure 1). The concentration of transferred oxygen ions is indicated based on the operating current. The influence of increasing current density on carbon deposition for biogas fuel ($R \geq 1.0$) is also shown in Figure 1. It is also claimed that carbon formation under operating condition (high current density) can be hydrogenated and removed from anode surface.[47]

However, there are two issues that should be addressed for the internal methane dry reforming in SOFC under closed-circuit operating conditions. The first major issue is that the kinetics of IDR is not very well known and very little attention has been paid to the role of CO_2 on methane conversion in the biogas fuelled SOFCs.[60] Chemical equilibrium condition might not be completely achieved inside the anode fuel channel because of the low residence time in contact with catalyst.[33] Understanding the kinetics of dry reforming can also help in suppressing thermal stress on the cell surface.[61] The second issue is attributed to the uniform distribution of fuel gas, steam, and CO_2 (generated through electrochemical reaction) on the anode surface. It should be considered that the distribution of current density is not uniform along the fuel channel inside the SOFC and increasing rapidly from the inlet of fuel channel, reaching to maximum in the middle and then decreasing again at the outlet.[62] Therefore, the risk of carbon deposition increases significantly at the inlet of fuel channel.

Experimental studies have shown the feasibility of biogas (60 mol.% methane) internal reforming for Ni-YSZ anode with a high concentration of H_2O (SC > 1.5) in fuel gas.[63] However, there is no agreement on additional CO_2 required for a safe long-term operation of biogas fuelled SOFCs. Moreover, the relative importance of current density is still debated and should be experimentally investigated.[28-30,36]

4 | EXPERIMENTAL

4.1 | Set up and cell specifications

Experimental research is adopted to investigate the feasibility of biogas internal dry reforming in an operational SOFC. A schematic of the experimental test bench is shown in Figure 2. Simulated gas is prepared by mixing the required gases stored in gas cylinders and the CH_4/CO_2 ratio (R) is adjusted by using mass flow controllers (MFC) (Bronkhorst High-Tech BV). The total flow rate of simulated gas for anode fuel is 1000 Nml min^{-1} and for the cathode side, air is simulated by mixing 1200 Nml min^{-1} nitrogen and 320 Nml min^{-1} oxygen. The anode inlet gas is preheated (by trace heating) to 120°C. Simulated air is also preheated inside the alumina tube which is exposed to the furnace electrical heaters and the off-gas is vented out to the environment. The anode outlet is also trace heated (130°C) in order to prevent steam condensation inside the pipe.

In this experimental study, the composition of the anode outlet gas is analyzed to calculate the methane conversion. A gas chromatograph (Agilent 490 microGC) device is used for this purpose. The anode outlet gas should be dried for this analysis in microGC columns (Molsieve 5A and PoraPLOT U). First, the anode outlet gas is bubbled through a steam condenser unit in order to remove steam and cooled down to the ambient temperature. It is then dried further in a silica gel bottle. A gas sample is then automatically taken by the MicroGC for analysis and the composition of the gas (dry based) is determined. It is considered that the silica gel adsorbs CO_2 at the beginning of the test and saturation time has been noted for sampling. A mass flow meter (MFM) (Bronkhorst High-Tech BV) is used for an indicative measurement of the flow rate of outlet gas to assess the gas leakage
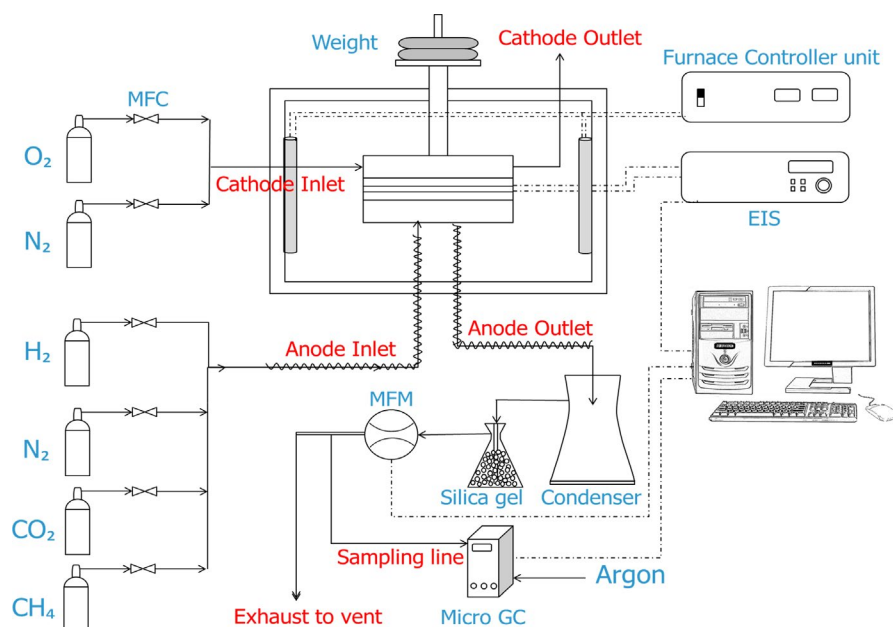

FIGURE 2 Schematic of the experimental test bench

in this setup. All electrochemical measurements, including the current-voltage (I-V) characterization, is performed in the potentiostatic control mode by an electronic impedance spectroscopy (EIS) device (Gamry FC-350). EIS measurements are also performed periodically in Galvanostatic mode to examine the electrochemical performance of the cell at different operating conditions.

Commercial planar Ni-GDC electrolyte-supported cells (ESC) manufactured by H.C Starck are used to conduct the experimental investigation on IDR at atmospheric pressure. This square cell consists of a 35 μm thick NiO-GDC (Ni-Gd$_{0.1}$ Ce$_{0.9}$ O$_{1.95}$) anode, 100 μm YSZ electrolyte, and a 40 μm LSM (La$_{1-x}$Sr$_x$MnO$_{3-\delta}$) cathode. The anode activated area is 81 cm^2 with about 57% wt. NiO and 23 wt.% cerium. The electrolyte area is 100 cm^2. The cell is placed between two alumina blocks and the gas tightness is achieved with a ceramic sheet in the anode side and a mica (thermiculite) sheet in the cathode side. To ensure the gas sealing, extra weight is added on the top of the block as shown in Figure 2. Anode off-gas flow rate can be measured by an MFM. Comparison of the anode flow rate and the expected flow rate (after reforming) shows the gas tightness of sealing. The expected flow rate of the anode can be calculated based on the nitrogen balance and equilibrium calculation (with FactSage software). Current collectors for the anode and cathode sides are nickel and platinum mesh respectively. The cell temperature is measured with a k-type thermocouple (RS PRO, −50°C/+1200°C), placed inside the anode block and very close (2 mm) to the anode surface.

4.2 | Experimental method

After preparing the setup, the furnace is heated up to 1000°C with a ramp rate of 40°C/hr while nitrogen is fed into the anode and cathode sides. After stabilization of the cell temperature at 950°C, the Nickel oxide in the anode is reduced to Nickel by hydrogen while simulated air is fed to the cathode. In this procedure, the concentration of hydrogen is gradually increased from 2% to 100% during 4 hours of operation. At the beginning of the test, pure hydrogen was fed to the cell and an I-V characterization test was performed as a reference, and the area-specific resistance (ASR)

was calculated around 1.5 Ω cm^2 at high current densities (1000 A m^{-2} ≤ CD ≤ 2500 A m^{-2}). The anode off-gas flow rate measured by the MFM showed that less than 10% hydrogen leakage takes place inside the setup (including the cell holder block, pipes, and the steam condenser).

Based on SOFC stack operating temperature in commercial systems, the experiments are carried out at three different cell temperature ranges, 900, 850, and 800°C. Since the heaters are positioned close to the four furnace walls and the cell holder is placed at its center, the cell temperature is around 60°C less than the furnace setpoint temperature. In these experiments, the furnace temperature is adjusted to obtain the desired operating temperature (900/850/800°C) with biogas fuelled in equimolar ratio (R = 1.0) at OCV and the furnace temperature is kept constant for each operating temperature. The cell is fed with CH$_4$, CO$_2$, and N$_2$ mixtures with different R (CH$_4$/CO$_2$) ratios. This ratio is varied between 0.6 and 1.5 to simulate both methane-rich and poor biogas. When the R ratio is 1.5, the gas composition is similar to both CO$_2$ predominant and CH4 predominant biogas. When the R ratio is 1.5, the gas composition is similar to the real biogas with 60% methane concentration. Changing the gas composition through R values of 0.6–1.5 resulted in a change in cell temperature by ±5°C in comparison to the biogas fed with equimolar composition. This is because of the change in the rate of the endothermic methane reforming reactions.

For different gas compositions, the flow rate of the main fuel (CH$_4$) and the total flow rate of fuel are kept constant in order to cancel the influence of residence time (Table 2). So, the N$_2$ gas is added to the biogas gas composition as an inert gas. Considering the geometry of the fuel channels of the ceramic block in the anode side and the porosity of the current collector ($\varphi = 0.5$), the residence time was 410 ms according to the total flow rate of 1000 Nml min^{-1}.

The I-V characterizations were performed from OCV to 0.6 V with a rate of 30 mA s^{-1}. All EIS measurements are carried out in the frequency range from 100 Hz to 0.1 Hz. In order to understand the influence of methane conversion on cell electrochemical performance, the anode off-gas was analyzed at OCV and under specific current densities between 500 and 2000 A m^{-2} with a current density interval of 500 A m^{-2}. The methane conversion (X_{CH4}) is calculated based on the carbon balance of outlet gas composition at different current densities.

TABLE 2 Anode inlet gas compositions for the total flow of 1000 Nml min^{-1}

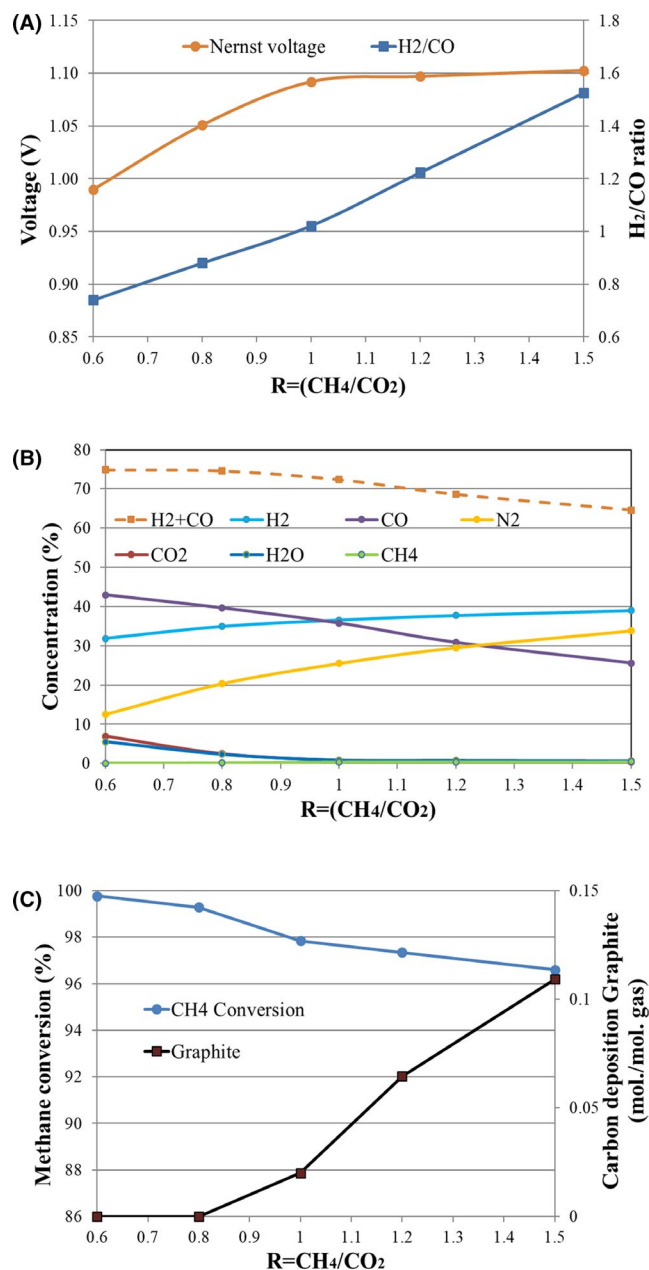| Gas composition	CH$_4$ (%)	CO$_2$ (%)	N$_2$ (%)	Total flow rate (Nml min^{-1})	R	O/C
A	30	50	20	1000	0.6	1.25
B	30	37.5	32.5	1000	0.8	1.11
C	30	30	40	1000	1.0	1.00
D	30	25	45	1000	1.2	0.91
E	30	20	50	1000	1.5	0.80

FIGURE 3 Equilibrium calculations at 850°C for different biogas compositions, (A) Nernst voltage and H_2/CO ratio, (B) reformed gas compositions, (C) methane conversion and carbon deposition at open-circuit voltage

Based on the methane (dry and steam) reforming reactions, one mole of methane produces in total four moles of CO and H_2. The H_2/CO ratio changes based on the operating condition due to the contribution of the RWGS reaction. Therefore, the methane conversion is calculated by the following Equation [64]

$$X_{CH_4} = \frac{Y_{CO} + Y_{H_2}}{4 \times Y_{CH_4} + Y_{CO} + Y_{H_2}} \quad (9)$$

where Y_i is the mole fraction of gas species i. It is important to mention that the concentration of the outlet gas was measured

when the operating conditions (the cell voltage and the cell temperature) were stabilized. This condition is obtained after 4 hours of cell operating at a certain gas composition, current density, and cell temperature. This is mainly because of stabilization of the cell temperature. The gas composition at the outlet was sampled and analyzed every 4 minutes.

5 | RESULTS AND DISCUSSION

In order to understand the influence of the CO_2 concentration on biogas-fed SOFC, Nernst voltage for different gas compositions has been calculated based on equilibrium conditions. The Nernst voltages for various inlet gases at 850°C are shown in Figure 3A. The Nernst voltage decreases with increasing the CO_2 concentration in the fuel (decreasing the R ratio). Adding CO_2 dilutes the fuel and the concentration of H_2 in the reformed gas decreases, which is shown in Figure 3B. Although the concentration of fuel (H_2 and CO) for SOFC in the reformed gas is higher with lower R ratios (Figure 3B), the Nernst voltage is lower. This is attributed to the low concentration of hydrogen and lower H_2/CO ratios for $R < 1$, as illustrated in Figure 3A. When the R ratio is more than one (equimolar CH_4/CO_2), the hydrogen partial pressure is higher than the CO.

The methane conversion at the equilibrium condition of 850°C is calculated by Equation (9). Methane conversion is higher than 96% for all gas compositions (Figure 3C) and it is above 99.7% when the R ratio is 0.6. Nevertheless, it is not possible to operate an SOFC for a long-term operation at OCV condition due to the carbon deposition for gas composition with low CO_2 concentrations ($R \geq 1.0$), as shown in Figure 3C based on the equilibrium condition.

5.1 | Influence of gas composition

Biogas-dry reforming experiments with various R ratios are conducted according to gas compositions in Table 2. First, the influence of gas composition on the performance of the cell has been investigated at 900°C. These tests have been conducted for a short period of time (around a half an hour) for each gas composition and repeated at 850 and 800°C as well.

The I-V characteristics for different gas compositions ($0.6 \leq R \leq 1.5$) at 850°C (the oven temperature) have been illustrated in Figure 4A. Results show that in short-term experiments, increasing the CO_2 concentration decreases the cell voltage for all current density ranges, as it is expected based on the thermodynamic calculations presented in Figure 3A. The OCV for gas composition with high concentration of CO_2 ($R = 0.6$) was higher (around 20 mV) than the calculated Nernst voltage shown in Figure 3A. This is attributed to the
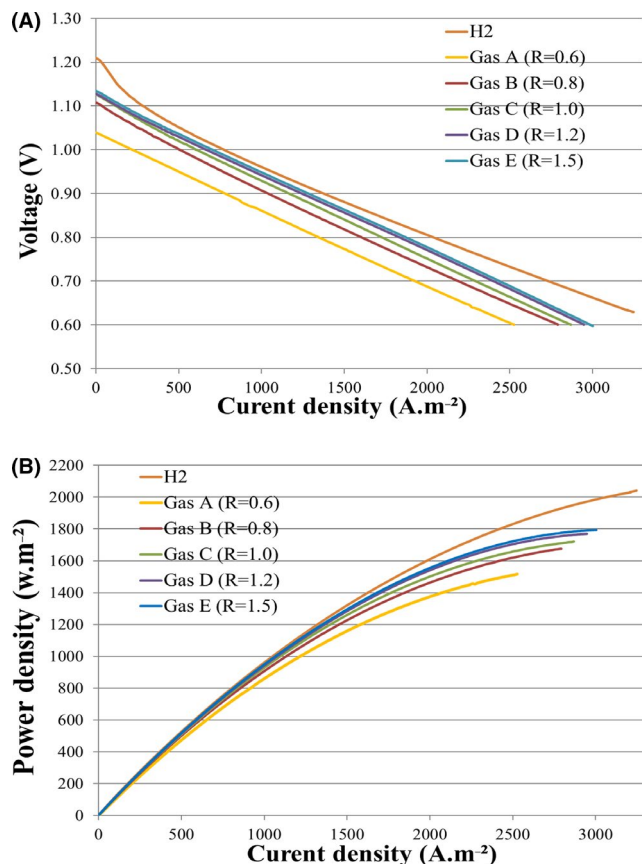
(A)

(B)

FIGURE 4 Influence of gas composition on the cell performance at different current densities at 850°C (A) the cell voltage, (B) the power density

(A)

(B)

FIGURE 5 Influence of gas composition and current density on (A) methane conversion (B) H_2/CO molar ratio at 850°C

lower cell temperature (840°C), because of the endothermic dry reforming reaction at higher partial pressure of CO_2 in biogas. The voltage difference between OCV and calculated Nernst voltage decreases (to a few mV) with the decreasing CO_2 concentration ($R \geq 1$). However, the ASR of the cell for all gas compositions was the same and with this short-term operation, there was no major degradation and increase of the cell resistance.

An I-V characteristic with pure H_2 fuel is also shown in Figure 4A as a reference. The ASR was slightly less for this test in comparison with biogas fuelled cell due to a higher cell operating temperature (858°C) and lower activation overpotential because of higher hydrogen concentration in the anode. Moreover, a relatively low concentration resistance was observed because of the higher H_2 concentration. The cell efficiency for the H_2 fed cell at the current density of 2000 A m^{-2}, was 63% ($E = 0.81$ V) and for the cell operating with the gas composition of $R = 1.0$ was 58.3% ($E = 0.75$ V).

The I-P characteristics are calculated for different gas compositions based on the results of the I-V characteristics and illustrated in Figure 4B. The power density decreases with increasing CO_2 concentrations. The power density of the cell fuelled with gas composition C ($R = 1.0$) is around
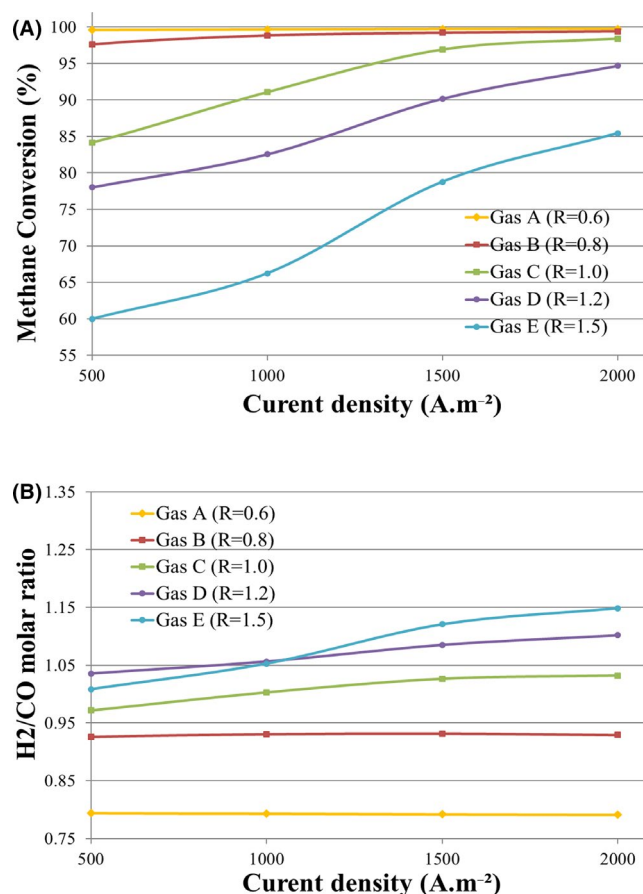
19% less than the hydrogen-fuelled one at a cell voltage of 0.7 V.

After I-V characterizations for different gas compositions, methane conversion has been studied for different R ratios at 850°C. Methane conversion at different current densities has been calculated based on the analyzed outlet gas compositions in order to understand the influence of gas composition and operating conditions on methane conversion. Considering the configuration of the setup, it takes 1 hour for each gas composition and current density to achieve stabilization (at a certain cell operating temperature), both in terms of the cell voltage and the gas compositions at the outlet. These tests have been conducted at current densities of 500–2000 A m^{-2} with an interval of 500 A m^{-2} since carbon deposition is predicted for gas composition E (biogas with $R = 1.5$) at OCV according to chemical equilibrium (see Figure 1).

Methane conversion is calculated by Equation (9) and shown in Figure 5A. Methane conversion increases by increasing CO_2 concentration at closed-circuit conditions. However, at high current densities, the methane conversion is above 95% for all gas compositions. For instance, methane conversion for gas compositions with $R \leq 1$ was the same at current density of 2000 A m^{-2} and increasing the
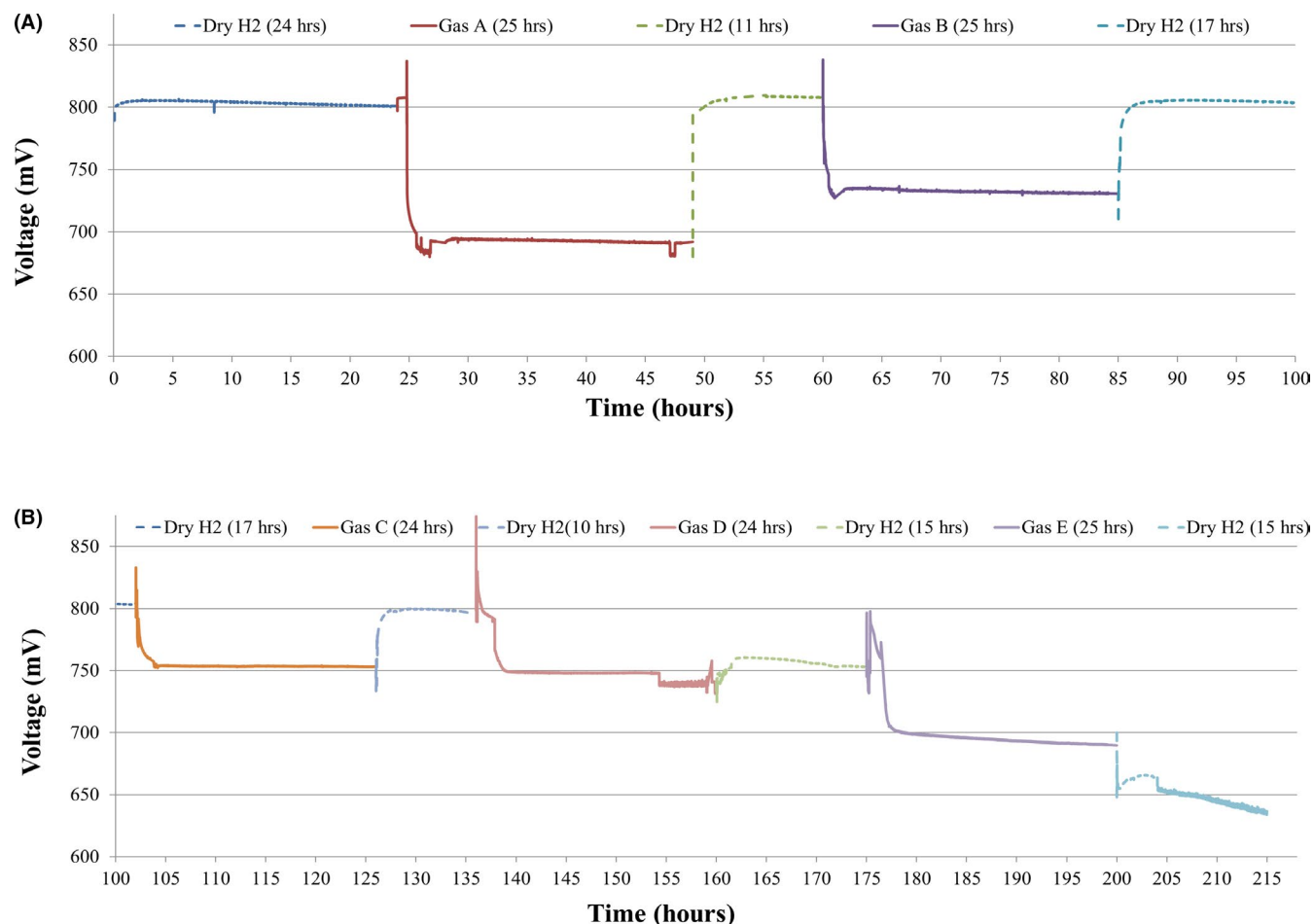
FIGURE 6 Cell stability testing results under hydrogen and various biogas compositions. (A) Gas composition *A*, *B*. (B) Gas composition *C*, *D,* and *E*, at a current density of 2000 A m^{-2} and 850°C

CO_2 concentration does not influence on the methane conversion rate. Analysis of the outlet gas shows that H_2 concentration at high current densities is higher (Figure 5B). Results are in agreement with equilibrium calculations shown in Figure 3A. For simulated biogas composition (*E*), the methane conversion is increased by 25% when the current density is increased to 2000 A m^{-2}.

It is claimed that the methane conversion is maximized for gas composition with *R* = 1.0 for a tubular cell[34] whereas, in this study, higher methane conversion is achieved with higher CO_2 concentration ($R \leq 1$) at open and closed-circuit conditions. During these tests, it is observed that rapidly changing the operating conditions (the CO_2 concentration and current density) increases the rate of cell degradation (dropping the cell voltage at a constant current density). This might be because of the thermal stress, which is due to endothermic (steam and dry) reforming reactions and the exothermic electrochemical reactions. This thermal stress can influence the anode electrolyte contact and increase the cell resistance. Therefore, for the rest of experimental tests, a current ramp of 5 mA/s is considered to increase and decrease the operating

current density. The CO_2 flow rate also is varied with a ramp of 5 ml/min.

5.2 | Cell degradation tests

During the short-term methane conversion tests in the previous section, it is noticed that the cell performance was degraded (cell voltage decreased at a constant current density) specifically for gas compositions *D* and *E*, with *R* > 1. In this section, cell degradation is investigated with a new cell placed inside the ceramic block. The test is conducted for all gas compositions mentioned in Table 2 at a current density of 2000 A m^{-2} and around 850°C (at constant furnace temperature). These conditions have been selected since biogas-SOFC stacks are commonly operated in this range of temperature ($800 < T < 850$°C) and the cell voltage ($0.6 < V < 0.8$). First, a reference test has been conducted with H_2/N_2 mixture with equivalent hydrogen (1200 Nml min^{-1}) similar to the biogas composition ($CH_4 = 300$ Nml min^{-1}). This is due to the fact that one mole of methane produces four moles of equivalent

hydrogen (H_2 and CO) regardless of either steam or dry reforming reactions taking place in the anode fuel channel.

The cell degradation with dry hydrogen at the current density of 2000 A m^{-2} has been monitored for 24 hours (see Figure 6A). The cell voltage is measured every 5 seconds. The cell temperature at this current density increased to 860°C and the cell degradation with this gas composition is attributed to normal aging of the anode (see Table 3). After measurement of the cell degradation rate with H_2, the cell is then fed with gas composition A at the same current density for 25 hours. Due to the endothermic reaction of methane reforming, the cell temperature decreased to 840°C which took approximately 1 hour to get it stabilized. The I-V and EIS measurements (at the current density of 2000 A m^{-2}) were conducted when the cell voltage stabilized. After roughly every 24 hours of operation at current density of 2000 A m^{-2}, the measurements were repeated in order to evaluate the cell electrochemical performance. Before changing the gas compositions to gas composition B, the experiment was continued by feeding dry hydrogen for 12 hours at the same current density in order to recover the cell electrochemical performance in case of a minor amount of carbon deposition (Figure 6A). I-V measurements were performed at the beginning and the end of each step. The same procedure at the current density of 2000 A m^{-2} was applied for all gas compositions mentioned in Table 2.

To the best of our knowledge, this is the first time that the cell voltage degradation under different dry reforming conditions (CO_2 concentration) has been reported as shown in Figure 6. It is important to mention that the I-V and EIS tests performed during the degradation experiments change the cell voltage. These parts of the experiment have not been shown in Figure 6.

During this experiment, the temperature of the furnace is kept constant. The cell temperature is higher with hydrogen in comparison with biogas fuels. The cell temperature drops due to the endothermic reforming reaction on the anode surface. The cell temperature influences the cell resistance and methane reforming rate. After changing the inlet fuel, it takes roughly 1 hour to reach a stable cell voltage. Different degradation rates were observed for different gas compositions (Table 3). Cell voltage fluctuation was observed for all gas compositions which was negligible (±1 mV) for gas composition C and D (only first 20 hours). The voltage fluctuation for gas compositions might be because of steam condensation in the anode outlet which causes a pressure gradient at the anode outlet pipe. The cell electrochemical performance was partially recovered after using H_2/N_2 gas mixture for gas composition A, B, and C. It should be noted that the part of the cell degradation is because of normal cell aging. For instance, the degradation rate (extrapolation of the short-term experiment) for hydrogen-fuelled cell was 0.125 V in 1000 hours. The cell voltage fluctuation for gas composition D was significant only at the end of the test period. The cell voltage suddenly dropped by 12 mV and started fluctuating. Changing the inlet gas composition to H_2/N_2 gas mixture could not improve the cell performance; however, the voltage stopped fluctuating after changing the gas composition to H_2/N_2 gas mixture. The cell voltage declined to 0.755 V with this gas mixture and dropped by 40 mV in comparison with the same gas composition before feeding composition D. In case of gas composition E (simulated biogas with 40% CO_2), the voltage fluctuation was not observed (less than ±3 mV) but, a continuous degradation rate occurred which was dramatically higher than other gas compositions.

The I-V characteristics for different gas compositions at the beginning and at the end of each period (see Figure 6) have been illustrated in Figure 7. For gas composition A with $R = 0.6$, negligible cell degradation was observed and the I-V curves before and after feeding gas composition A were identical (see Figure 7A). The cell degradation for gas composition B ($R = 0.8$) for 25 hours test at similar conditions was minor as it is shown in Figure 7A. In comparison with the cell voltage at initial phase, at high current densities, the cell voltage at the end of the 25-hour operation was only 10 mV lower than at the beginning of the test with the gas composition B. Subsequently, for gas composition C with equimolar CH_4 and CO_2, the cell degradation is in the same order of that for Gas B (though slightly lower), which is attributed to normal cell aging. The cell voltage at OCV for the final I-V curve of gas composition C is slightly (3 mV) higher than the initial one (Figure 7A), this might be because of a small amount of carbon deposition, which was reversible and did not influence on the cell performance during the long-term experiment. The ASR of the cell operating with different gas compositions is calculated based on the I-V curve measurements at the beginning of each test and shown in Table 3. The higher ASR for gas composition D and E, could be related to the lower concentration of H_2 and CO in the reformed gas.

As discussed at the beginning of this subsection, a sudden cell degradation was observed for gas D after 20 hours operation under the current density of 2000 A m^{-2}. The influence

TABLE 3 Cell degradation rates and ASR for different biogas compositions under current density of 2000 A m^{-2} at 850°C

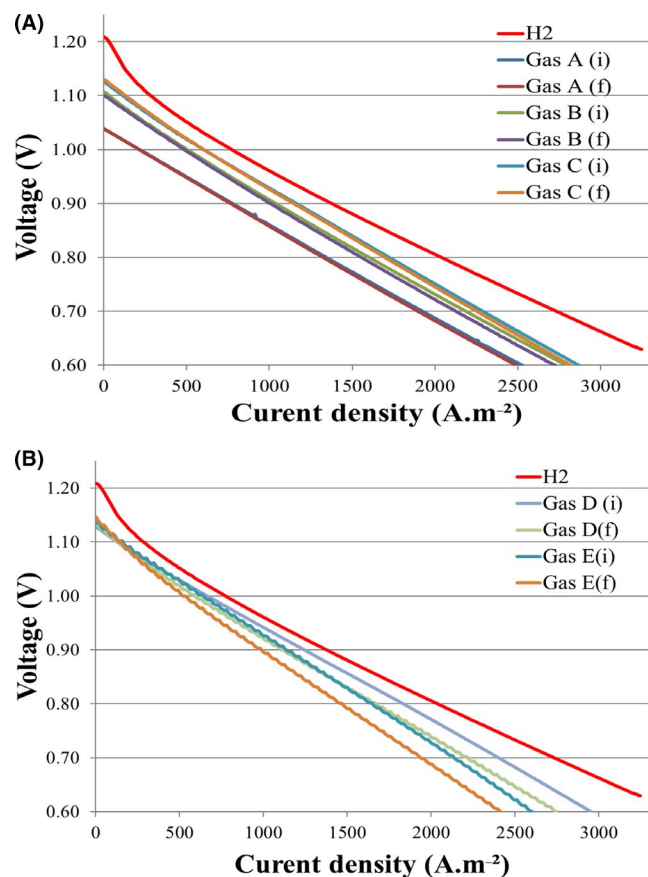| Gas compositions	Hydrogen	Gas A	Gas B	Gas C	Gas D	Gas E
Degradation rates (V/1000 h)	0.125	0.16	0.16	0.14	0.625	0.630
ASR (Ω cm^2)	1.52	1.71	1.73	1.74	1.76	1.98

(A)

(A)

(B)

(B)

FIGURE 7 The I-V characteristics, for the cell stability test under hydrogen and various biogas (0.6 < R < 1.5) (A) Gas composition A, B, and C. (B) Gas composition D and E, at 850°C (i: Initial, f: Final)

FIGURE 8 The EIS measurements, for the cell stability tests under various biogas compositions (0.6 < R < 1.5) (A) Gas composition A, B. (B) Gas composition C, D, and E, under current density of 2000 A m^{-2} at 850°C

of voltage fluctuation (with a tendency to decrease the voltage) is also visible on the I-V characterization after relatively long-term experiment (see Figure 7B). The current density achieved at 0.6 V was 250 A m^{-2} less than the beginning of the long-term test. In the case of gas composition E (simulated biogas), the voltage fluctuation of ±5 mV was observed during the whole experiment period. The degradation at the end of this experiment was also in the same order of degradation for gas composition D. Increasing the cell voltage at OCV after the 25 hours experiment for gas compositions D and E might be because of the solid carbon oxidation at the high operating temperature which is generated during the relatively long-term test. This is more visible in gas composition E in Figure 7B.

Figure 8 shows the measured electrochemical impedance spectra (EIS) for gas compositions with various R ratios measured between 100 and 0.1 Hz, before and after relatively long-term experiments, operated at 850°C. A steady current density of 2000 A m^{-2} was imposed in all EIS measurements. The intercept with the real axis at high frequency in the left-side of Nyquist arcs corresponds to the purely ohmic resistance of the cell. The low frequency in the right side is activation and mass transfer losses due to the gas conversion,
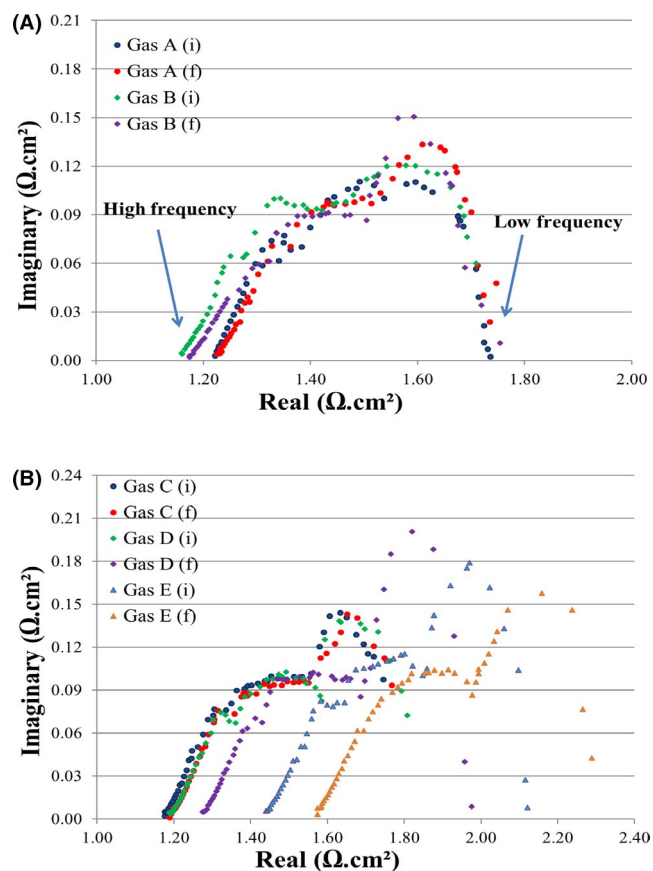
diffusion, and oxidation through the electrodes. Carbon deposition causes a gradual filling of the anode porosity, which depresses the charge transfer process and results in higher losses. In Figure 8, the shape of arcs showed only minor changes by varying the fuel composition. Low-frequency experimental data were found to be slightly noisy, which is because of the gas transport limitation.

Decreasing the CO$_2$ concentration in the fuel gas increases the cell temperature due to less endothermic dry reforming. This leads to a higher electrolyte cell ionic conductivity and the Nyquist curve shifts to the left at high-frequencies (Figure 8A). This should be mentioned that the cell temperature increases (roughly 5°C) by decreasing CO$_2$ concentration from gas composition A to B. The ohmic resistance is higher for gas compositions D and E. This could be because of the lower methane conversion and lower H$_2$ and CO concentrations (as already shown in Figure 5A) at the current density of 2000 A m^{-2}.

After relatively long-term experiments, the high-frequency intercept shifts to the right for all gas compositions, meaning higher resistance, which is negligible for gas composition A, B, and C (Figure 8A). This is partially attributed to normal cell aging for the gas compositions with R ≤ 1.0. The cell

resistance increases dramatically after the relatively long-term experiment for gas compositions *D* and *E* (Figure 8B). This is mainly attributed to cell degradation due to carbon deposition. A gradual filling of the anode porosity impacts the charge transfer process and results in higher losses in low frequency. This results in a decrease in the active triple phase boundary (TPB) area. The formation of carbon fibers can result in the removal of Ni particles from the electrode. This occurs when the nickel catalyst is physically lifted from the electrode by its attachment to the growing carbon fibers. Ni delamination reduces the electrolyte ionic conductivity and thereby increases the cell ohmic resistance, as observed in Figure 8B.

After this long-term experiment, the furnace was cooled down, and the cell was taken out of the furnace. Anode delamination and nickel reoxidation were observed on the anode surface close to the fuel inlet (Figure 9). Carbon deposition occurred at the fuel inlet when $R > 1$, although a safe operation was predicted based on chemical equilibrium calculations at a current density of 2000 A m^{-2} (Figure 1). This is in agreement with the findings of Baldinelli et al[65] and Yong Jiao et al.[66]

5.3 | Influence of cell temperature

In order to evaluate the influence of operating temperature on cell electrochemical performance, the same I-V and methane conversion measurements have been conducted for gas composition *C* (with equimolar CH$_4$ and CO$_2$) at different current densities at 900 and 800°C as well. This gas composition is

selected because the produced power was maximum during the degradation test (See Figure 6). The methane conversion of gas composition *C* at the chemical equilibrium condition (at 850°C) is around 98%. Decreasing the cell temperature, substantially decreases the methane conversion.[67] After obtaining a stable performance of SOFC fuelled by gas composition *C*, the methane conversion for this gas composition at different current densities has been investigated at different operating temperatures and illustrated in Figure 10A. At OCV, the methane conversion increases by 23% by increasing the operating temperature from 800 to 900°C. However, at high current densities (2000 A m^{-2}), the difference is negligible, around 5%. This shows that a high methane conversion (97%) is achieved at the operating of 850°C and high current density (2000 A m^2), and a further increase in operating temperature is not required to obtain a high methane conversion.

The H$_2$/CO ratio of the outlet gas for different operating temperatures is shown in Figure 10B. At OCV (when there is no steam produced through the electrochemical reaction of hydrogen), the H$_2$/CO ratio is less than one for all operating temperatures. Increasing the operating temperature more than 850°C (at OCV) promotes the methane reforming, but this does not improve the H$_2$/CO ratio anymore as it is observed in Figure 10B.
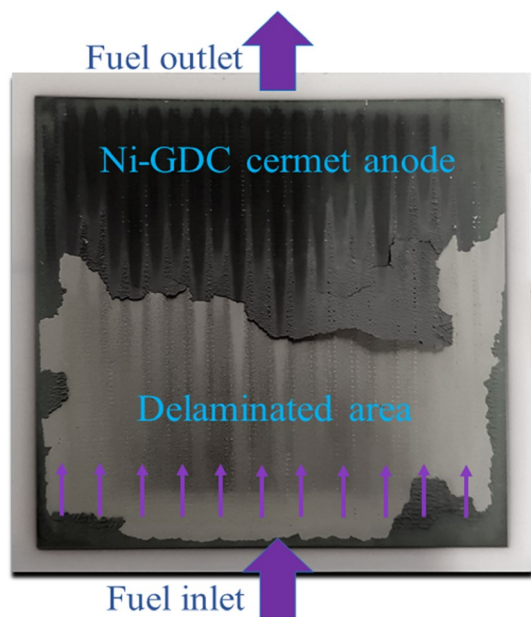

FIGURE 9 A photo of the anode side of cell operated under biogas internal dry reforming with various biogas compositions $(0.6 < R < 1.5)$ after the long-term experiment
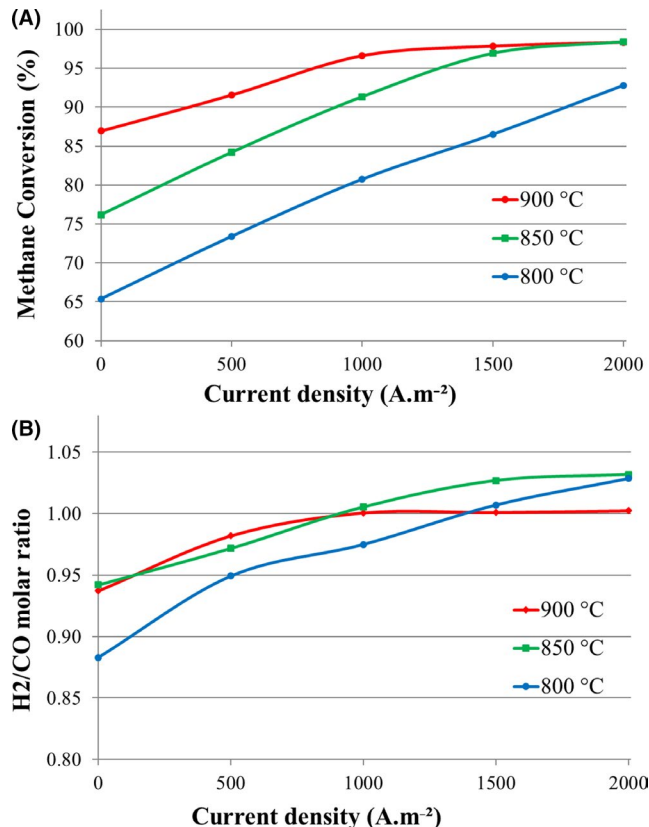

FIGURE 10 Influence of operating temperature on (A) methane reforming (B) H$_2$/CO ratio for gas composition *C* ($R = 1$)

At a low operating temperature (800°C), the H_2/CO ratio increases by increasing the current density. However, increasing the current density does not affect the H_2/CO ratio for the cell operating at 900°C and current densities above 1000 A m^{-2}. At this temperature, the methane reforming is already high, and increasing the current density does not change the methane reforming rate (see Figure 10A).

Moreover, the cell temperature also influences the cell electrochemical performance which increases the conductivity of the cell electrolyte, and this reduces the ohmic losses within the cell.[59] At higher operating temperatures, higher current densities can be achieved with the same gas composition. Impact of the cell temperature on the performance of the cell fed with gas composition C has been shown in Figure 11.

For hydrogen-fed SOFCs, the OCV is normally lower at a higher operating temperature, according to the Nernst equation. However, for biogas fuelled SOFC, the OCV at higher operating temperature is higher. This is because of a higher rate of methane dry reforming and a higher concentration of H_2 and CO. It should be emphasized that operation at high temperature (above 900°C) increases the aging (degradation) rate of electrolyte due to loss of ionic conductivity.[68,69] Thus, it is not advised to increase the cell temperature even though a higher current density can be achieved. Moreover, for SOFC stacks, cell sealing is more challenging at high operating temperature.

5.4 | Influence of residence time

In this section, the influence of residence time on methane conversion and electrochemical performance of cell was investigated. These experiments were conducted for gas composition C with different inlet flow rates (20% higher and lower than reference test) and residence time (Table 4) at 850°C and different current densities.

The outlet gas composition (dry-based) was analyzed by the MicroGC. Increasing the residence time by decreasing
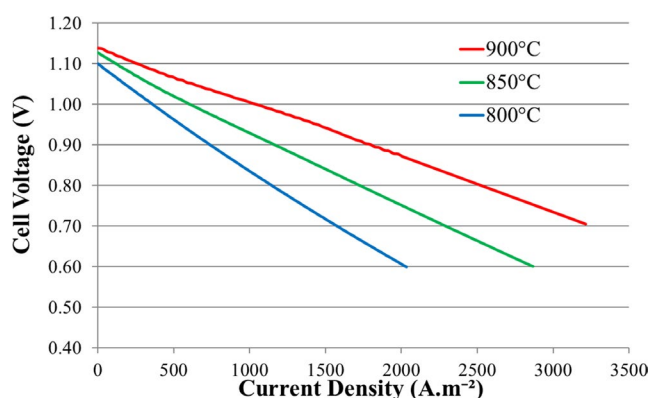

FIGURE 11 The I-V characteristics, influence of operating temperature on the cell performance for gas composition C

the total flow rate increases the methane conversion as shown in Figure 12. Decreasing the residence time from 512 ms *(C-1)* to 410 ms *(C-2)* does not impact on methane conversion dramatically. However, decreasing the residence time to 340 ms *(C-3)* decreases the methane conversion by roughly 5%, which is also in the same range for high and low current densities. Results showed that using a longer residence time *(C-1)* can slightly promote the methane conversion; however, this is limited by fuel utilization (U_f). It is advised to keep the overall U_f around 80% in the SOFC stack operation.

The I-V characterizations of this gas composition with different flow rates (different residence times) have been illustrated in Figure 13. Higher cell voltage and higher current density have been achieved with longer residence time due to a higher methane conversion. However, the difference is negligible. In these experiments at a current density of 2000 A m^{-2}, the fuel utilization was around 19% at a methane flow rate of 300 Nml min^{-1} (gas composition *C-2*). Decreasing the fuel utilization by increasing the inlet flow rate, can decrease the cell voltage and power production at higher current densities due to decreasing the methane conversion rate. This has not been seen in this experiment since the residence time was long enough for these gas compositions.
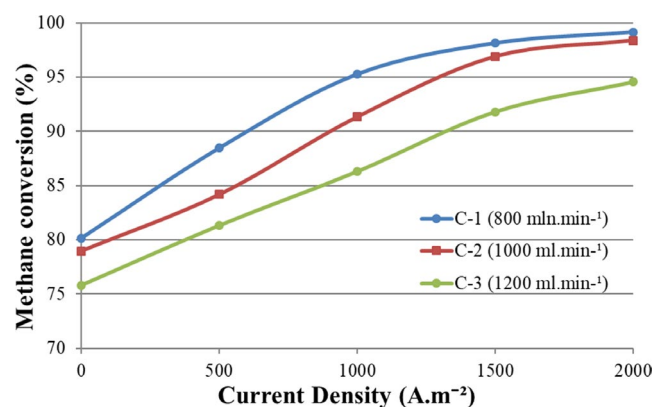
6 | CONCLUSIONS

Internal dry reforming of biogas in electrolyte-supported solid oxide fuel cell, with a Ni-GDC anode has been studied at different operating conditions. After preliminary thermochemical equilibrium prediction of carbon deposition for specific gas compositions and conditions, experimental investigations were conducted. One of the main objectives of this study was to determine the minimum amount of extra CO_2 required to obtain maximum power density at stable cell performance (in comparison to hydrogen-fuelled one) and at the same time prevent carbon deposition.

Complete characterization of biogas-SOFC with different CH_4/CO_2 molar ratios ($0.6 < R < 1.5$) has been performed for short-term studies in order to understand the influence of CO_2 concentration and current density on methane conversion. Methane conversion increases by increasing CO_2 concentration. Steam produced through electrochemical reaction of hydrogen impacts the methane reforming when $R \geq 1$ and the methane conversions were above 95% for all gas compositions at a current density of 2000 A m^{-2}. However, a high degradation rate has been observed with simulated biogas (with 60 mol.% methane) fed, due to carbon deposition at 850°C. In this experiment, carbon deposition led to an anode Ni re-oxidation and delamination of the cell surface close to the fuel inlet. Furthermore, the results showed that changing the residence time does not significantly influence methane conversion at 850°C. This implies that the kinetics of the

TABLE 4 Anode inlet gas compositions and inlet flow rate for different residence times at 850°C

Gas composition	CH_4 (%)	CO_2 (%)	N_2 (%)	R	Total flow rate (Nml min^{-1})	U_f (@ 2000 A m^{-2})	Residence time (ms)
C-1	30	30	40	1	800	0.24	512
C-2	30	30	40	1	1000	0.19	410
C-3	30	30	40	1	1200	0.16	340

FIGURE 12 Influence of residence time and current density on methane conversion at 850°C
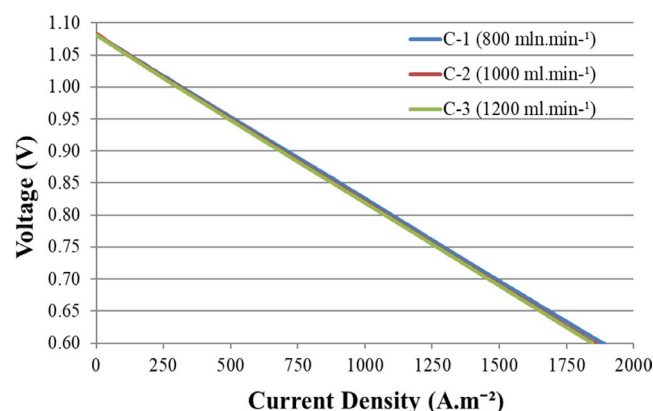
FIGURE 13 The I-V characteristics, influence of operating temperature on the cell performance

reforming reactions is fast enough for the internal reforming of methane.

Continuous, relatively long-term operation (more than 215 hours) under a current density of 2000 A m^{-2} has been conducted for gas compositions with different CO_2 concentrations. This represents the novelty of this research on direct dry reforming of methane with a Ni-GDC anode (with a commercial cell size). Stable cell performance (in terms of voltage decrease at constant current density) has been achieved when $R \leq 1$ and carbon deposition observed when $R > 1$. The best performance has been achieved with $R = 1$ since the degradation was minimum and power production was

maximized. With this R ratio, more than 97% of the methane reformed at a current density of 2000 A m^{-2}, and the highest H_2/CO molar ratio was achieved in comparison with SOFC fuelled with safe operating condition ($R \leq 1$). However, biogas-fuelled SOFC system's power density is around 19% less than hydrogen-fuelled one, and this should be considered while designing the biogas-SOFC system.

NOMENCLATURE

Acronyms

AD	Anerobic Digestion
ASC	Anode Supported Cell
ASR	Area specific resistance
CHP	Combined heat and power
CD	Current density
DIR	Direct internal reforming
EIS	Electrochemical impedance spectroscopy
ESC	Electrolyte-supported cell
GC	Gas chromatograph
GCU	Gas cleaning unit
GDC	Gadolinium-doped ceria
IC	Internal combustion
IDR	Internal dry reforming
LHV	Lower heating value
LSM	Lanthanum strontium manganite
MFC	Mass flow controller
MFM	Mass flow meter
OCV	Open-circuit voltage
RWGS	Reverse water gas shift
SC	Steam to carbon ratio
ScSZ	Scandia-stabilized zirconia
SOFC	Solid oxide fuel cell
TPB	Triple phase boundary
VOC	Volatile organic compound
WGS	Water-gas shift
WWTP	Wastewater treatment plants
YSZ	Yttria-stabilized zirconia

Greek letters

ΔG	Gibbs free energy change of reaction, (kJ mol^{-1})
ΔH	Enthalpy change of reaction, (kJ mol^{-1})
η_{cell}	Cell efficiency (%)

Symbols

F	Faraday constant (C/mol)
I	Current (A)
n	Number of electrons participating in the electrochemical reactions (–)
P	Power (W)
$P_{O_2\,cat}$	Equilibrium oxygen partial pressure at cathode
$P_{O_2\,ano}$	Equilibrium oxygen partial pressure at cathode
R	Universal gas constant (J/mol K)
T	Temperature (°C)
U_f	Fuel utilization (%)
V_{cell}	Cell voltage (V)
V_{Nernst}	Nernst voltage (V)
X_{CH4}	Methane conversion (%)
Y_i	mole fraction of gas species i (–)

ORCID

S. Ali Saadabadi https://orcid.org/0000-0001-5056-139X

REFERENCES

1. Hosseini SE, Wahid MA. Feasibility study of biogas production and utilization as a source of renewable energy in Malaysia. _Renew Sustain Energy Rev_. 2013;19:454-462.
2. Scarlat N, Dallemand J-F, Fahl F. Biogas: developments and perspectives in Europe. _Renewable Energy_. 2018;129:457-472.
3. Gude VG. Energy and water autarky of wastewater treatment and power generation systems. _Renew Sustain Energy Rev_. 2015;45:52-68.
4. de Arespacochaga N, Valderrama C, Mesa C, Bouchy L, Cortina JL. Biogas deep clean-up based on adsorption technologies for Solid Oxide Fuel Cell applications. _Chem Eng J_. 2014;255:593-603.
5. Lanzini A, Gandiglio M, Papurello D, Santarelli M. DEMOnstration of large SOFC system fed with biogas from WWTP; 2016.
6. Papurello D, Boschetti A, Silvestri S, Khomenko I, Biasioli F. Real-time monitoring of removal of trace compounds with PTR-MS: biochar experimental investigation. _Renewable Energy_. 2018;125:344-355.
7. Shen Y, Linville JL, Urgun-Demirtas M, Mintz MM, Snyder SW. An overview of biogas production and utilization at full-scale wastewater treatment plants (WWTPs) in the United States: challenges and opportunities towards energy-neutral WWTPs. _Renew Sustain Energy Rev_. 2015;50:346-362.
8. Porpatham E, Ramesh A, Nagalingam B. Investigation on the effect of concentration of methane in biogas when used as a fuel for a spark ignition engine. _Fuel_. 2008;87:1651-1659.
9. Van Herle J, Maréchal F, Leuenberger S, Favrat D Energy balance model of a SOFC cogenerator operated with biogas. _J Power Sources_. 2003;118:375-383.
10. Saadabadi SA, Thallam Thattai A, Fan L, Lindeboom REF, Spanjers H, Aravind PV. Solid Oxide Fuel Cells fuelled with biogas: potential and constraints. _Renewable Energy_. 2019;134:194-214.
11. Maréchal F, Leuenberger S, Membrez Y, Bucheli O, Favrat D. Process flow model of solid oxide fuel cell system supplied with sewage biogas. _J Power Sources_. 2004;131:127-141.

12. Henshaw PF, D'Andrea T, Mann KR, Ting DS-K. Premixed ammonia-methane-air combustion. _Combust Sci Technol_. 2005;177:2151-2170.
13. Farhad S, Yoo Y, Hamdullahpur F. Effects of fuel processing methods on industrial scale biogas-fuelled solid oxide fuel cell system for operating in wastewater treatment plants. _J Power Sources_. 2010;195:1446-1453.
14. Trendewicz A, Braun R. Techno-economic analysis of solid oxide fuel cell-based combined heat and power systems for biogas utilization at wastewater treatment facilities. _J Power Sources_. 2013;233:380-393.
15. de Arespacochaga N, Valderrama C, Peregrina C, Mesa C, Bouchy L, Cortina J. Evaluation of a pilot-scale sewage biogas powered 2.8 kW e Solid Oxide Fuel Cell: assessment of heat-to-power ratio and influence of oxygen content. _J Power Sources_. 2015;300:325-335.
16. Barelli L, Ottaviano A. Solid oxide fuel cell technology coupled with methane dry reforming: a viable option for high efficiency plant with reduced CO2 emissions. _Energy_. 2014;71:118-129.
17. Sasaki K, Haga K, Yoshizumi T, et al. Impurity poisoning of SOFCs. _ECS Trans_. 2011;35:2805-2814.
18. Papurello D, Chiodo V, Maisano S, Lanzini A, Santarelli M. Catalytic stability of a Ni-Catalyst towards biogas reforming in the presence of deactivating trace compounds. _Renewable Energy_. 2018;127:481-494.
19. Lanzini A, Ferrero D, Papurello D, Santarelli M. Reporting degradation from different fuel contaminants in Ni-anode SOFCs. _Fuel Cells_. 2017;17:423-433.
20. Tjaden B, Gandiglio M, Lanzini A, Santarelli M, Jarvinen M. Small-scale biogas-SOFC plant: technical analysis and assessment of different fuel reforming options. _Energy Fuels_. 2014;28:4216-4232.
21. Papurello D, Lanzini A, Tognana L, Silvestri S, Santarelli M. Waste to energy: exploitation of biogas from organic waste in a 500 Wel solid oxide fuel cell (SOFC) stack. _Energy_. 2015;85:145-158.
22. Ormerod RM. Solid oxide fuel cells. _Chem Soc Rev_. 2003;32:17-28.
23. Liese EA, Gemmen RS. Performance comparison of internal reforming against external reforming in a solid oxide fuel cell, gas turbine hybrid system. _J Eng Gas Turbines Power_. 2005;127:86-90.
24. Van Biert L, Godjevac M, Visser K, Aravind P. Dynamic modelling of a direct internal reforming solid oxide fuel cell stack based on single cell experiments. _Appl Energy_. 2019;250:976-990.
25. Park MH, Choi BK, Park YH, Moon DJ, Park NC, Kim YC. Kinetics for steam and CO2 reforming of methane over Ni/La/Al2O3 catalyst. _J Nanosci Nanotechnol_. 2015;15:5255-5258.
26. Chiodo V, Galvagno A, Lanzini A, et al. Biogas reforming process investigation for SOFC application. _Energy Convers Manage_. 2015;98:252-258.
27. Shiratori Y, Ijichi T, Oshima T, Sasaki K. Internal reforming SOFC running on biogas. _Int J Hydrogen Energy_. 2010;35:7905-7912.
28. Lanzini A, Leone P. Experimental investigation of direct internal reforming of biogas in solid oxide fuel cells. _Int J Hydrogen Energy_. 2010;35:2463-2476.
29. Yentekakis IV, Papadam T, Goula G. Electricity production from wastewater treatment via a novel biogas-SOFC aided process. _Solid State Ionics_. 2008;179:1521-1525.

30. Goula G, Kiousis V, Nalbandian L, Yentekakis IV. Catalytic and electrocatalytic behavior of Ni-based cermet anodes under internal dry reforming of CH4+CO2 mixtures in SOFCs. *Solid State Ionics*. 2006;177:2119-2123.

31. Pillai M, Lin Y, Zhu H, Kee RJ, Barnett SA. Stability and coking of direct-methane solid oxide fuel cells: effect of CO 2 and air additions. *J Power Sources*. 2010;195:271-279.

32. Staniforth J, Ormerod RM. Implications for using biogas as a fuel source for solid oxide fuel cells: internal dry reforming in a small tubular solid oxide fuel cell. *Catal Lett*. 2002;81:19-23.

33. Santarelli M, Quesito F, Novaresio V, Guerra C, Lanzini A, Beretta D. Direct reforming of biogas on Ni-based SOFC anodes: modelling of heterogeneous reactions and validation with experiments. *J Power Sources*. 2013;242:405-414.

34. Yentekakis IV. Open-and closed-circuit study of an intermediate temperature SOFC directly fueled with simulated biogas mixtures. *J Power Sources*. 2006;160:422-425.

35. Girona K, Laurencin J, Fouletier J, Lefebvre-Joud F. Carbon deposition in CH4/CO2 operated SOFC: simulation and experimentation studies. *J Power Sources*. 2012;210:381-391.

36. Xu J, Zhou W, Li Z, Wang J, Ma J. Biogas reforming for hydrogen production over a Ni–Co bimetallic catalyst: effect of operating conditions. *Int J Hydrogen Energy*. 2010;35:13013-13020.

37. Lanzini A, Leone P, Guerra C, Smeacetto F, Brandon NP, Santarelli M. Durability of anode supported Solid Oxides Fuel Cells (SOFC) under direct dry-reforming of methane. *Chem Eng J*. 2013;220:254-263.

38. Guerra C, Lanzini A, Leone P, Santarelli M, Brandon NP. Optimization of dry reforming of methane over Ni/YSZ anodes for solid oxide fuel cells. *J Power Sources*. 2014;245:154-163.

39. Ouweltjes J, Aravind P, Woudstra N, Rietveld G. Biosyngas utilization in solid oxide fuel cells with Ni/GDC anodes. *J Fuel Cell Sci Technol*. 2006;3:495-498.

40. Zhang L, Jiang SP, He HQ, Chen X, Ma J, Song XC. A comparative study of H2S poisoning on electrode behavior of Ni/YSZ and Ni/GDC anodes of solid oxide fuel cells. *Int J Hydrogen Energy*. 2010;35:12359-12368.

41. Mahato N, Banerjee A, Gupta A, Omar S, Balani K. Progress in material selection for solid oxide fuel cell technology: a review. *Prog Mater Sci*. 2015;72:141-337.

42. Jablonski WS, Villano SM, Dean AM. A comparison of H2S, SO2, and COS poisoning on Ni/YSZ and Ni/K2O-CaAl2O4 during methane steam and dry reforming. *Appl Catal A*. 2015;502:399-409.

43. Johnson GB, Hjalmarsson P, Norrman K, Ozkan U, Hagen A. Biogas catalytic reforming studies on nickel-based solid oxide fuel cell anodes. *Fuel Cells*. 2016;16:219-234.

44. Staniforth J, Ormerod RM. Running solid oxide fuel cells on biogas. *Ionics*. 2003;9:336-341.

45. Ni M. Is steam addition necessary for the landfill gas fueled solid oxide fuel cells? *Int J Hydrogen Energy*. 2013;38:16373-16386.

46. Hong SK, Dong SK, Han JO, Lee JS, Lee YC. Numerical study of effect of operating and design parameters for design of steam reforming reactor. *Energy*. 2013;61:410-418.

47. Chen T, Wang WG, Miao H, Li T, Xu C. Evaluation of carbon deposition behavior on the nickel/yttrium-stabilized zirconia anode-supported fuel cell fueled with simulated syngas. *J Power Sources*. 2011;196:2461-2468.

48. Alenazey F, Alyousef Y, Brancaccio E, Montinaro D. Parameters affecting CO2 production in a planar anode supported SOFC based system. *Int J Hydrogen Energy*. 2015;40:642-651.

49. Papurello D, Borchiellini R, Bareschino P, et al. Performance of a Solid Oxide Fuel Cell short-stack with biogas feeding. *Appl Energy*. 2014;125:254-263.

50. Xuan J, Leung MKH, Leung DYC, Ni M. A review of biomass-derived fuel processors for fuel cell systems. *Renew Sustain Energy Rev*. 2009;13:1301-1313.

51. Lavoie J-M. Review on dry reforming of methane, a potentially more environmentally-friendly approach to the increasing natural gas exploitation. *Front Chem*. 2014;2:1-17.

52. Ashrafi M, Pröll T, Pfeifer C, Hofbauer H. Experimental study of model biogas catalytic steam reforming: 1. Thermodynamic optimization. *Energy Fuels*. 2008;22:4182-4189.

53. Rosha P, Mohapatra SK, Mahla SK, Dhir A. Hydrogen enrichment of biogas via dry and autothermal-dry reforming with pure nickel (Ni) nanoparticle. *Energy*. 2019;172:733-739.

54. Chen W-H, Lin M-R, Jiang TL, Chen M-H. Modeling and simulation of hydrogen generation from high-temperature and low-temperature water gas shift reactions. *Int J Hydrogen Energ*. 2008;33:6644-6656.

55. Callaghan CA. *Kinetics and catalysis of the water-gas-shift reaction: A microkinetic and graph theoretic approach*. 2006.

56. Laosiripojana N, Assabumrungrat S. Catalytic dry reforming of methane over high surface area ceria. *Appl Catal B*. 2005;60:107-116.

57. Assabumrungrat S, Laosiripojana N, Piroonlerkgul P. Determination of the boundary of carbon formation for dry reforming of methane in a solid oxide fuel cell. *J Power Sources*. 2006;159:1274-1282.

58. Dietrich RU, Oelze J, Lindermeir A, Spieker C, Spitta C, Steffen M. Power generation from biogas using SOFC–results for a 1 kWe demonstration unit. *Fuel Cells*. 2014;14:239-250.

59. Larminie J, Dicks A, McDonald MS. *Fuel Cell Systems Explained*, Vol. 2. New York: Wiley; 2003.

60. Lanzini A, Leone P, Pieroni M, Santarelli M, Beretta D, Ginocchio S. Experimental investigations and modeling of direct internal reforming of biogases in tubular solid oxide fuel cells. *Fuel Cells*. 2011;11:697-710.

61. Mogensen D, Grunwaldt J-D, Hendriksen PV, Dam-Johansen K, Nielsen J. Internal steam reforming in solid oxide fuel cells: status and opportunities of kinetic studies and their impact on modelling. *J Power Sources*. 2011;196:25-38.

62. Fan L, Qu Z, Pourquie M, Verkooijen A, Aravind P. Computational studies for the evaluation of fuel flexibility in solid oxide fuel cells: a case with biosyngas. *Fuel Cells*. 2013;13:410-427.

63. Madi H, Diethelm S, Petigny N. Effect of steam-to-carbon ratio on degradation of Ni-YSZ anode supported cells. *ECS Trans*. 2013;57:1517-1525.

64. Gokon N, Osawa Y, Nakazawa D, Kodama T. Kinetics of CO2 reforming of methane by catalytically activated metallic foam absorber for solar receiver-reactors. *Int J Hydrogen Energy*. 2009;34:1787-1800.

65. Baldinelli A, Barelli L, Bidini G, Di Michele A, Vivani R. SOFC direct fuelling with high-methane gases: optimal strategies for fuel dilution and upgrade to avoid quick degradation. *Energy Convers Manage*. 2016;124:492-503.

66. Jiao Y, Zhang L, An W, et al. Controlled deposition and utilization of carbon on Ni-YSZ anodes of SOFCs operating on dry methane. *Energy*. 2016;113:432-443.

67. Lee WY, Hanna J, Ghoniem AF. On the predictions of carbon deposition on the nickel anode of a SOFC and its impact on open-circuit conditions. *J Electrochem Soc*. 2012;160:F94.

68. Jacques-Bédard X, Napporn T, Roberge R, Meunier M. Performance and ageing of an anode-supported SOFC operated in single-chamber conditions. *J Power Sources*. 2006;153:108-113.

69. Laurencin J, Roche V, Jaboutian C, Kieffer I, Mougin J, Steil M. Ni-8YSZ cermet re-oxidation of anode supported solid oxide fuel cell: from kinetics measurements to mechanical damage prediction. *Int J Hydrogen Energ*. 2012;37:12557-12573.